







A quasi single-phase model for debris flows and its comparison with a two-phase model

XIA Chun-chen*  <http://orcid.org/0000-0002-8984-7085>;  e-mail: xcc@whu.edu.cn

LI Ji¹  <http://orcid.org/0000-0003-4328-3197>; e-mail: lijimy0321@whu.edu.cn

CAO Zhi-xian¹  <http://orcid.org/0000-0001-5161-385X>; e-mail: zxcao@whu.edu.cn

LIU Qing-quan²  <http://orcid.org/0000-0002-4472-6626>; e-mail: liuqq@bit.edu.cn

HU Kai-heng³  <http://orcid.org/0000-0001-8114-5743>; e-mail: khhu@imde.ac.cn

* Corresponding author

¹ State Key Laboratory of Water Resources and Hydropower Engineering Science, Wuhan University, Wuhan 430072, China

² Department of Mechanics, School of Aerospace Engineering, Beijing Institute of Technology, Beijing 100081, China

³ Institute of Mountain Hazards and Environment, Chinese Academy of Sciences, Chengdu 610041, China

Citation: Xia CC, Li J, Cao ZX, et al. (2018) A quasi single-phase model for debris flows and its comparison with a two-phase model. *Journal of Mountain Science* 15(5). <https://doi.org/10.1007/s11629-018-4886-5>

© Science Press, Institute of Mountain Hazards and Environment, CAS and Springer-Verlag GmbH Germany, part of Springer Nature 2018

Abstract: A depth-averaged quasi single-phase mixture model is proposed for debris flows over inclined bed slopes based on the shallow water hydro-sediment-morphodynamic theory with multi grain sizes. The stresses due to fluctuations are incorporated based on analogy to turbulent flows, as estimated using the depth-averaged $k - \varepsilon$ turbulence model and a modification component. A fully conservative numerical algorithm, using well-balanced slope limited centred scheme, is deployed to solve the governing equations. The present quasi single-phase model using four closure relationships for the bed shear stresses is evaluated against USGS experimental debris flow and compared with traditional quasi single-phase models and a recent physically enhanced two-phase model. It is found that the present quasi single-phase model performs much better than the traditional models, and is attractive in terms of computational cost while the two-phase model performs even better appreciably.

Keywords: Debris flows; Quasi single-phase mixture model; Stresses due to fluctuations; Well-balanced

Notation:

c_k, C_T = size-specific and total sediment concentration;

c_{ek} = size-specific sediment concentration at capacity;

C_f = friction coefficient;

C_r = Courant number;

$C_\mu, C_{\varepsilon 1}, C_{\varepsilon 2}, C_\Gamma$ = coefficients in the $k - \varepsilon$ model;

d_k = the diameter of the k th size sediment;

d_m = mean sediment diameter;

d_{84} = the particle size at which 84% of the sediment are finer;

D_k, D_T = size-specific and total sediment deposition flux;

E_k, E_T = size-specific and total sediment entrainment flux;

f_{ak}, f_{sk}, f_{lk} = fraction of the k th size sediment in the active layer, substrate layer and the interface between

Received: 07 February 2018

Revised: 20 March 2018

Accepted: 12 April 2018

the active layer and substrate layer respectively;

F_k = the areal exposure fraction of k th sediment on the bed surface;

F_{skf} , F_{ssk} = the size-specific depth-averaged interphase interaction force and particle–particle interaction drag force, respectively;

\mathbf{F} = vector of flux variables;

g = gravitational acceleration;

$g_z = g \cos \gamma$;

h , h_s , h_f = debris flow depth, the thickness of the solid and fluid phases, respectively;

\hat{h} , \hat{W} , \hat{u} = the normalized flow depth, channel width, and mixture flow velocity respectively;

i_{sk} , i_f = velocity differences;

i , j = spatial and time node index;

j_s = friction slope;

l = the mixing length;

L^1 = norm to quantify the difference;

M = coefficient in line with ψ ;

n = Manning roughness;

n' = Manning roughness corresponding to the grain resistance;

k = depth-averaged fluctuation kinetic energy;

p = bed sediment porosity;

P_k , P_{kb} , P_{eb} = production terms;

q_k = size-specific transport rate at capacity regime;

R_{pk} , R_{p0} = particle Reynolds numbers to compute m_k and m_0 respectively;

t = time;

T_R , T_{Rsk} = depth-averaged stress due to fluctuations of the mixture flows and the size-specific solid phase;

T_0 , T_A = depth-averaged stress due to fluctuations closed by $k - \varepsilon$ model and modification component respectively;

T_μ , $T_{\mu sk}$ = depth-averaged viscous stress for the mixture flows and the size-specific solid phase, respectively;

u_* = friction velocity;

U , U_{sk} , U_f = depth-averaged flow velocity, size-specific solid phase velocity, and fluid phase velocity, respectively;

U_w = a characteristic velocity for the onset of dramatic weakening;

\mathbf{U} = vector of conservative variables;

$s = \rho_s / \rho_f - 1$;

S_G , S_{TR} = gravitational term, stress term due to fluctuation;

S_{T0} , S_{TA} = components of stress terms due to fluctuation;

\mathbf{S}_b , \mathbf{S}_f , \mathbf{S}_d = vectors of source terms;

x = streamwise coordinate;

x_f , x_f^* = computed and measured flow front location;

m_k , m_0 = exponents of the closure for sediment deposition flux;

z_b = bed elevation;

α = empirical coefficient in modification component;

χ = a material coefficient of order unity;

γ = bed slope angle;

Δt = time step;

Δx = spatial step;

δ = thickness of the active layer;

ε = depth-averaged fluctuation dissipation rate;

η = water level;

η_k = hiding and exposure factor;

θ = water content of the bed;

λ_k = empirical parameter;

λ_{\max} = maximum celerity;

μ_0 = static friction coefficient;

μ_w = thermally weakened friction coefficient;

$\bar{\mu}$ = the tangent of the angle of repose of the dry granular material in absence of lateral confinement;

μ_s = the coefficient of sliding friction;

ν_μ = kinematic viscosity of water;

ν_t = depth-averaged eddy viscosity;

ξ = elevation of the bottom surface of the active layer;

ρ , ρ_0 = density of water-sediment mixture and the bed;

ρ_s , ρ_f = densities of solid and fluid phases respectively;

σ = modification coefficient;

σ_k , σ_ε = coefficients in the $k - \varepsilon$ model;

τ = shear stress at channel cross-section;

τ_b = bed shear stress for the debris flow;

τ_{ck} = size-specific critical shear stress;

τ_{bf} , τ_{bs} = bed shear stress of the fluid and solid phases;

τ_{bsk} = bed shear stresses of the size-specific solid phase;

Φ_b = the friction angle of the solid phase;

ω_k = size-specific settling velocity;

ϕ = empirical weighting parameter; and

ψ = variables representing U , k and ε .

Introduction

Debris flows are fast landslide earth movements with highly concentrated mixtures of sediments and water (Ancey 2001; Takahashi 2007; Cardoso-Landa 2009), which commonly occur in mountainous areas around the world. Different triggering mechanisms contribute to the inception of debris flows (Cascini et al. 2013), and one of the most common causes is rainfall (Iverson 2000; Guadagno et al. 2005; Cascini et al. 2008; Jeng and Sue 2016). Debris flows generally happen when large quantities of poorly sorted sediments, agitated and saturated with water, surge down steep slopes in response to the gravitational effects (Iverson 1997). The entrainment due to scour of bed materials or collapse of stream banks may contribute to increasing debris-flow volume by even several orders of magnitude before deposition begins on flatter terrain downstream (Berti et al. 1999; Santi et al. 2008; Berger et al. 2011; Iverson et al. 2011). They gain high speed and great destructive power, which are particularly dangerous for the life and properties throughout their trajectories. Examples of the catastrophic debris flow disasters reported in the recent decades are the 1999 Vargas State debris flow in Venezuela that killed more than 30 thousand people (Wei et al. 2000), and the 2010 Zhouqu debris flow in China which caused 1765 death (Cui et al. 2013). Analysis and prediction are therefore of great importance for hazard assessment and guidance to authorities and people in coping with such disasters.

Numerical simulations are key tools in studying the catastrophic processes of debris flows and in the prediction of disaster occurrence under complicated conditions. While fully three-dimensional modelling may facilitate very detailed resolution of the phenomena, the excessively high computing cost makes it unrealistic to be applied to large-scale cases. Comparatively, depth-averaged models based on mass and momentum conservation feature a sensible balance between theoretical integrity and applicability and therefore have seen widespread applications. Most mathematical models can be clarified as the quasi single-phase mixture models (Takahashi 1991; Iverson 1997; Brufau et al. 2000; Denlinger and Iverson 2001; Pudasaini et al. 2005; Armanini et al. 2009; Rosatti and Begnudelli 2013) and the two-

phase models (Pitman and Le 2005; Pelanti et al. 2008; Pailha and Pouliquen 2009; Pudasaini 2012; Greco et al. 2012; Cozzolino et al. 2014; Bouchut et al. 2015; Di Cristo et al. 2016; D'Aniello et al. 2015; Meng and Wang 2016). The main difference between the two kinds of models is that the former is characterized by a single momentum equation for mixture flow, assuming the same velocity of fluid and solid phases, while the later has separate momentum equation for each solid phase, considering the different velocities for each phase. The two-phase model is attractive because it can explicitly reveal the relative motions and interactions between the fluid and solid phases. But accordingly, the increase in computing costs and also the demand for extra relationships to close the governing equations constrain its applications. Moreover, it is still unclear if they can perform considerably better than traditional quasi single-phase models in terms of modelling accuracy (Cao et al. 2017). Although quasi single-phase models are widely used, most of them still suffer from some shortcomings. For example, some models were decoupled, neglecting the interactions between the flow, sediment transport and morphological evolution (Denlinger and Iverson 2001; Liu and Huang 2006), which confined their applications to fixed bed cases; some were based on the capacity assumption that sediment concentration was assumed to be always equal to its transport capacity (Armanini et al. 2009; Rosatti and Begnudelli 2013), which may not be generally justified from physical perspectives (Cao et al. 2012; Cao et al. 2016). From mathematical perspective, the stresses due to fluctuations is derived by time-averaging the original full three dimensional momentum conservation equations. But most models were restricted to uniform sediment transport cases and generally ignored the effects of debris flows fluctuations (Shieh et al. 1996; Brufau et al. 2000; Hotta et al. 2015). It is known that roll waves is a readily observed phenomenon in experimental debris flows by Iverson et al. (2010) and roll waves are ubiquitous in debris flows (Zanuttigh and Lamberti 2007; Balmforth and Liu 2004; Di Cristo et al. 2015). The research on roll waves of clear water by Cao et al. (2015) demonstrated that the effects of turbulent stresses are considerable in water roll waves as large-scale vortexes arise behind the shocks.

Physically, the solid and fluid phases are generally well mixed along the depth when debris flow is developed, and thus it is hard to identify a pure fluid layer over a solid-fluid mixture layer. But it is worth mentioning that more sophisticated two-layer depth-averaged models have been recently proposed for better describing the rheological stratification in granular mixtures and immature debris flows (Armanini et al. 2005; Luca et al. 2009; Sarno et al. 2014; Sarno et al. 2017; Meng et al. 2017). Comparatively, approximated models such as kinematic or diffusive wave one (Chiang et al. 2012; Gregoretti et al. 2016; Rengers et al. 2016) along with their applicability criteria (Di Cristo et al. 2014; Di Cristo et al. 2018) are used to simplify complicated debris flow models for improving computational efficiency.

It is well recognized that numerical modelling is fundamentally based on sound physical understandings. But debris flow dynamics involves a number of extremely complicated mechanisms, e.g. random interphase and particle-particle interactions, strong fluctuations of the fluid and solid motions, substantial mass growth due to bed erosion and particle segregation, which to date remain poorly understood (Hutter et al. 1994; Coussot and Meunier 1996; Iverson 1997). Fortunately, the last several decades have witnessed the great efforts taken by researchers to conduct their investigations by both field observations (Okuda et al. 1977; Rickenmann and Zimmermann 1993; Berti et al. 1999; Hürlimann et al. 2003; McArdell et al. 2007; Imaizumi et al. 2016) and laboratory experiments (Di Silvio and Gregoretti 1997; Parsons et al. 2001; Mangeney et al. 2010; Hürlimann et al. 2015; Hu et al. 2016), which provide considerable insights into the physics of debris flows. Most notably, a series of experiments, including both fixed and erodible bed cases, conducted at large-scale U.S. Geological Survey (USGS) debris flow flume. A systematic set of observed data that are well-suited for validating mathematical models of debris flows were presented along with a detailed analysis on the theoretical aspects (Iverson et al. 1997; Iverson et al. 2010; Iverson et al. 2011).

This paper focuses on the one-dimensional depth-averaged quasi single-phase mixture model with non-uniform sediment transport to simulate the debris flow evolution over inclined bed slopes

under the framework of the shallow water hydro-sediment-morphodynamic model (Cao et al. 2004, 2017). On the basis of the work of Cao et al. (2015) about roll waves of clear water over steep slopes, the stresses due to fluctuations of debris flows are considered and analogous to turbulent flows. They are determined by the depth-averaged $k-\varepsilon$ turbulence model along with a modification component. A fully conservative numerical algorithm (Xia et al. 2017), using well-balanced weighted surface depth gradient method (WSDGM) version of the slope limited centred (SLIC) scheme (Aureli et al. 2008), is deployed to solve the governing equations. The present quasi single-phase model with four bed stresses closure formulas is evaluated by the experimental data of the USGS large-scale debris flows over both fixed bed (Iverson et al. 2010) and erodible bed (Iverson et al. 2011), and compared with the performance of the traditional quasi single-phase models by George and Iverson (2014) and Ouyang et al. (2015) and the two-phase model by Li et al. (2017a, b). The effects of stresses due to fluctuations of the quasi single-phase model and the sensitivities of the involved coefficients are also assessed.

1 Governing Equations

The depth-averaged quasi single-phase equations (QSPE) can be derived from the conservation laws under the framework of shallow water hydro-sediment-morphodynamics. And the detailed derivation of the depth-averaged governing equations is given in Supplementary (Appendix 1). For one-dimensional debris flows over an inclined erodible bed composed of non-cohesive sediment with N size classes (d_k denotes the diameter of the k th size sediment and $k = 1, 2, \dots, N$), the governing equations comprise the mass and momentum conservation equations for the fluid-solid (water-sediment) mixture, the size-specific mass conservation equations for the solid phase, the total mass conservation equation for the solid phase in the bed as well as the size-specific mass conservation equations for the solid phase in the active layer based on the widely used three-layer structure (i.e., bed load layer, active layer and substrate layer) (Hirano 1971). They can be written as follows

$$\frac{\partial \rho h}{\partial t} + \frac{\partial \rho h U}{\partial x} = -\rho_0 \frac{\partial z_b}{\partial t} \quad (1)$$

$$\frac{\partial \rho h U}{\partial t} + \frac{\partial}{\partial x} \left(\rho h U^2 + \frac{1}{2} \frac{g_z}{\rho} (\rho h)^2 \right) = \rho h g \sin \gamma - \rho h g_z \frac{\partial z_b}{\partial x} - \tau_b + \frac{\partial h (T_R + T_\mu)}{\partial x} \quad (2)$$

$$\frac{\partial (\rho_s h c_k)}{\partial t} + \frac{\partial (\rho_s h U c_k)}{\partial x} = \rho_s (E_k - D_k) \quad (3)$$

$$\frac{\partial z_b}{\partial t} = -\frac{E_T - D_T}{1 - p} \quad (4)$$

$$\frac{\partial \delta f_{ak}}{\partial t} + f_{lk} \frac{\partial \xi}{\partial t} = \frac{(D_k - E_k)}{1 - p} \quad (5)$$

where t = time; x = streamwise coordinate parallel to bed slope with the angle γ ; h = debris flow depth; U = depth-averaged mixture flow velocity in x direction; z_b = bed elevation; c_k = depth-averaged size-specific volumetric sediment concentration and $C_T = \sum c_k$ = total sediment concentration; g = gravitational acceleration and $g_z = g \cos \gamma$; τ_b = bed shear stress; p = bed sediment porosity; ρ_f, ρ_s = densities of fluid and solid phases respectively; $\rho = \rho_f(1 - C_T) + \rho_s C_T$ = density of fluid-solid mixture; $\rho_0 = \rho_f \theta + \rho_s(1 - p)$ = density of the bed, and θ = water content of the bed ($\theta \leq p$); E_k = size-specific sediment entrainment flux and $E_T = \sum E_k$ = total sediment entrainment flux; D_k = size-specific sediment deposition flux and $D_T = \sum D_k$ = total sediment deposition flux; δ = thickness of the active layer and $\delta = 2d_{84}$, where d_{84} is the particle size at which 84% of the sediment are finer; f_{ak} = fraction of the k th size sediment in the active layer; $\xi = z_b - \delta$ = elevation of the bottom surface of the active layer; f_{lk} = fraction of the k th size sediment in the interface between the active layer and substrate layer; T_R = depth-averaged stress due to fluctuations of debris flows in the x direction; and T_μ = depth-averaged viscous stress of debris flows in the x direction.

As the erosion process plays a key role in flow dynamics and should be included in debris flow models, the present model is fully coupled, explicitly accommodating the mass exchange between the flow and the bed, as is shown on the right-hand side (RHS) of Eq. (1). Meanwhile, a non-capacity approach is used, which determines the size-specific sediment transport by incorporating the contributions of advection due to

mean flow velocity and of the mass exchange with the bed (Eq. (3)).

The depth-averaged two-phase model, according to Li et al. (2017a, b), takes into consideration the difference in velocity between the fluid and solid phases, as well as the mass and momentum conservation for the size-specific solid phase. Accordingly, besides the same mixture flow mass conservation equation (Eq. (1)), bed deformation equation (Eq. (4)) and active layer equation (Eq. (5)), the momentum conservation equation for the mixture and the mass and momentum conservation equations for the solid phase can be written as

$$\frac{\partial \rho h U}{\partial t} + \frac{\partial}{\partial x} \left(\rho h U^2 + \frac{1}{2} \rho g_z h^2 \right) = \rho h g \sin \gamma - \rho h g_z \frac{\partial z_b}{\partial x} - \tau_b \quad (6)$$

$$+ \frac{\partial h (T_R + T_\mu)}{\partial x} - \frac{\partial h \sum [\rho_s c_k i_{sk} (i_{sk} - i_f)]}{\partial x} \quad (7)$$

$$\frac{\partial (\rho_s h c_k)}{\partial t} + \frac{\partial (\rho_s h U_{sk} c_k)}{\partial x} = \rho_s (E_k - D_k) \quad (7)$$

$$\frac{\partial \rho_s h c_k U_{sk}}{\partial t} + \frac{\partial}{\partial x} \left(\rho_s h c_k U_{sk}^2 + \frac{1}{2} c_k \rho g_z h^2 \right) = \rho_s h c_k g \sin \gamma - \rho h c_k g_z \frac{\partial z_b}{\partial x} - \tau_{bsk} + F_{skf} + F_{ssk} \quad (8)$$

where $i_{sk} = U_{sk} - U$, $i_f = U_f - U$ = differences among the size-specific solid phase velocity U_{sk} , fluid phase velocity U_f and the mixture flow velocity U ; τ_{bsk} = bed shear stress for the size-specific solid phase; T_{Rsk} = depth-averaged stress due to fluctuations of solid motions; $T_{\mu sk}$ = depth-averaged viscous stress for the size-specific solid phase; and F_{skf} = the size-specific depth-averaged interphase interaction force; F_{ssk} = the size-specific depth-averaged particle-particle interaction drag force, which is exerted on the k th size sediment by the other constituents of solid phase and $\sum F_{ssk} = 0$.

It can be seen that the last term in the RHS of Eq. (6) indicates the different velocities among the size-specific solid phase, fluid phase and the mixture flow. The size-specific solid phase velocity U_{sk} in the second term in LHS (left hand side) of Eq. (7) is different from its counterpart U in Eq. (3) which represents the mixture velocity. The additional momentum conservation equation for

size-specific solid phase (Eq. (8)) provides insight into the solid phase motions, establishing a sounder governing equation system from the physical perspective.

2 Model Closures

The present quasi single-phase model needs to be closed by introducing a set of relationships for the bed shear stresses, sediment exchange fluxes and stresses due to the fluctuations of debris flows. While the closure models for the depth-averaged two-phase model can be obtained by Li et al. (2017a, b).

2.1 Bed shear stress

Bed shear stress is rather complicated to model as it is related to the rheological properties of debris flows, which depend on various factors, such as sediment concentration, particle shape and grain size distribution (Imran et al. 2001). The last several decades have witnessed the development of different relationships to represent the boundary resistances for debris flows that are used by researchers, for example, Newtonian models (Hunt 1994), Bagnold’s models (Armanini et al. 2009), Bingham models (O’Brien 1986), Herschel-Bulkley models (Laigle and Coussot 1997) and frictional models (Iverson 1997; Savage and Hutter 1989; Gray et al. 1999; Sarno et al. 2013). Here, for non-cohesive sediments, the total bed shear stress for the debris flow is considered to be composed of bed shear stresses exerted on the fluid phase τ_{bf} and solid phase τ_{bs} respectively, which reads

$$\tau_b = \tau_{bf} + \tau_{bs} \tag{9}$$

Four closure models for the bed shear stresses are employed to evaluate their effects on modelling. The notations are summarized in Table 1.

Table 1 Summary of the closure models for the bed shear stresses

| Notations | Solid shear stress | Fluid shear stress |
|-----------|------------------------------|------------------------|
| CM | Coulomb friction law | Manning’s equation |
| BM | Berzi–Larcán formula | Mixing length approach |
| LM | Lucas et al. formula | Manning’s equation |
| RLM | Revised Lucas et al. formula | Manning’s equation |

In the Coulomb-Manning (CM) closure model, the Coulomb friction law is used to determine the solid shear stress (Savage and Hutter 1989; Egashira 2011), with a friction coefficient to express the collinearity of shear and normal stresses. Thus, the solid phase resistance can be obtained as

$$\tau_{bs} = \rho_s g_z h_s \tan \Phi_b \hat{m}_b \text{sgn}(U) \tag{10}$$

where $h_s = h(1 - C_T)$ is the thickness of the solid phase; Φ_b = the friction angle of the solid phase; and $\hat{m}_b = \sqrt{1 + (\partial z_b / \partial x)^2}$. For the fluid phase resistance, the conventional empirical relation for the fluvial processes is used, which involves the Manning roughness n

$$\tau_{bf} = \rho_f g_z h_f \frac{n^2 U^2}{h_f^{4/3}} \hat{m}_b \tag{11}$$

where $h_f = h C_T$ is the thickness of the fluid phase.

In the Berzi–Larcán - Mixing length (BM) closure model, the friction slope j_s , proposed by Berzi and Larcán (2013), is derived analytically under uniform conditions for debris flows. It is used to estimate the bed shear stress exerted on the solid phase.

$$\tau_{bs} = \rho_s g_z h_s j_s \tag{12}$$

$$j_s = \frac{s C_T}{s C_T + 1} \bar{\mu} + \frac{5\chi}{2} \left[\frac{s(s+1)^{1/2} C_T}{(s C_T + 1) \cos \theta^{1/2}} \left[\frac{\hat{u}}{\hat{h}^{3/2}} + \frac{2 s^{1/2} \cos \theta^{1/2}}{7\chi (s+1)^{1/2}} \frac{\hat{h}}{\hat{W}} \mu_s \right] \right] \tag{13}$$

where $s = \rho_s / \rho_f - 1$; $\bar{\mu}$ = the tangent of the angle of repose of the dry granular material in absence of lateral confinement; χ = a material coefficient of order unity; μ_s = the coefficient of sliding friction; $\hat{h} = h / d_m$, $\hat{W} = W / d_m$, $\hat{u} = U / \sqrt{g d_m}$ = the normalized flow depth, channel width, and mixture flow velocity respectively; and $d_m = \sum (c_k d_k) / C_T$ means sediment diameter. The bed shear stress exerted on the fluid phase is estimated by a mixing length approach (Berzi and Jenkins 2008)

$$\tau_{bf} = \rho_f (1 - C_T) l^2 (dU / dz) \tag{14}$$

$$\frac{dU}{dz} = \frac{1}{\chi} \left[\frac{s C_T + 1}{s C_T} \tan \theta - \frac{h}{W} \mu_s - \bar{\mu} \right] \left[\frac{s \cos \theta}{(s+1)} \right]^{1/2} \frac{\sqrt{gh}}{d_m} \tag{15}$$

where l = the mixing length and can be taken to be

roughly one-tenth of the mean diameter d_m (Berzi and Larcán 2013).

In the Lucas - Manning (LM) and Revised Lucas-Manning (RLM) closure model, Lucas et al. (2014) found an empirical relationship between the effective friction coefficient μ_e and the flow velocity, which is analogous to the basic flash weakening theory (Rice 2006; Beeler et al. 2008), which is employed to estimate the solid phase resistance.

$$\tau_{bs} = \rho_s g_s h_s \mu_e \hat{m}_b \operatorname{sgn}(U) \quad (16)$$

$$\mu_e(U) = \frac{\mu_0 - \mu_w}{1 + \|U\|/U_w} + \mu_w \quad (17)$$

where μ_0 = static friction coefficient; μ_w = thermally weakened friction coefficient; U_w = a characteristic velocity for the onset of dramatic weakening. According to Lucas et al. (2014), the complicated conditions could span a broad range for the possible values of the parameters μ_0 , μ_w and U_w , in particular of U_w . In the LM model, the constant empirical parameters suggested by Lucas et al. (2014) would be directly used. While in the RLM model, $\mu_0 = \tan \Phi_b$ to express the static friction coefficient changing with bed conditions, and U_w is expected for the individual test case. The fluid shear stress for both LM and RLM closure model is estimated by Manning's equation (Eq. (11)).

2.2 Sediment entrainment and deposition

Sediment entrainment due to fluctuations and sediment deposition by gravitational action are two distinct mechanisms involved in mass exchange with the bed, which are still poorly understood. Generally, the deposition flux can be computed by the local near-bed sediment concentration and the hindered settling velocity. And the entrainment flux is mostly based on the assumption that entrainment always occurs at the same rate as it does under capacity regime. Empirically, the size-specific sediment entrainment and deposition fluxes are estimated as

$$E_k = \lambda_k \omega_k c_{ek} \quad (18)$$

$$D_k = \lambda_k \omega_k c_k (1 - c_k)^{m_k} (1 - C_T)^{m_0} \cos \theta \quad (19)$$

where ω_k = size-specific settling velocity computed by the formula of Zhang and Xie (1993); and λ_k = empirical parameter representing the difference between the near-bed sediment concentration and

the depth-averaged sediment concentration. Physically, the water and sediments are generally well mixed along the depth of debris flows, thus $\lambda_k = 1$ is used. The hindered effects on sediment settling in deposition flux come from the water as well as the sediments of other size fractions. According to Richardson and Zaki (1954), $m_k = 4.45 R_{pk}^{-0.1}$, $R_{pk} = \omega_k d_k / \nu_\mu$, $m_0 = 4.45 R_{p0}^{-0.1}$, R_{p0} is determined by the mean sediment diameter d_m , and ν_μ is the kinematic viscosity of water. The size-specific sediment concentration at capacity c_{ek} is calculated as

$$c_{ek} = F_k q_k / (hU) \quad (20)$$

where q_k = size-specific transport rate at capacity regime and the formula of Wu et al. (2000) is adopted. In the processes of the incipient motion and movement of non-uniform sediments, the coarse grains are easier to be entrained than their counterparts in uniform cases because they have higher exposure chance to flow, while fine grains are more difficult to be entrained as they are more likely to be sheltered by coarse grains, which is known as the hiding and exposure effect. Thus F_k is the areal exposure fraction of k th sediment on the bed surface given by Parker (1991)

$$F_k = \frac{f_{ak} / \sqrt{d_k}}{\sum (f_{ak} / \sqrt{d_k})} \quad (21)$$

According to Wu et al. (2000), each sediment size is transported as bed load and suspended load at the same time. Therefore, sediment transport rate of k th sediment can be determined as

$$\begin{aligned} & \frac{q_k}{\sigma \sqrt{(\rho_s / \rho_f - 1) g_s d_k^3}} \\ &= 0.0053 \left[\left(\frac{n'}{n} \right)^{1.5} \frac{\tau_b}{\tau_{ck}} - 1 \right]^{2.2} + 0.0000262 \left[\left(\frac{\tau}{\tau_{ck}} - 1 \right) \frac{U}{\omega_k} \right]^{1.74} \end{aligned} \quad (22)$$

where σ = modification coefficient; $n' = d_{50}^{1/6} / 20$ = Manning roughness corresponding to the grain resistance; τ = shear stress at channel cross-section; $\tau_{ck} = 0.03 \eta_k (\rho_s - \rho_f) g_s d_k$ = size-specific critical shear stress, and η_k = hiding and exposure factor computed by Wu et al. (2000).

In order to solve the Eq. (5), an empirical relation to evaluate f_{lk} is needed to be introduced (Hoey and Ferguson 1994; Cui et al. 1996).

$$f_{lk} = \begin{cases} f_{sk} & \partial \xi / \partial t \leq 0 \\ \phi C_k / C_T + (1 - \phi) f_{ak} & \partial \xi / \partial t > 0 \end{cases} \quad (23)$$

where f_{sk} = fraction of the k th size sediment in the substrate layer; ϕ = empirical weighting parameter, and $\phi = 0.7$ is used according to [Toro-Escobar et al. \(1996\)](#).

2.3 Stresses due to fluctuations and viscosity

To date, the generally applicable closure models for fluctuations of debris flows remain unavailable. [Iverson et al. \(2010\)](#) pointed out that roll waves are a ubiquitous, readily measured phenomenon in each of the USGS experimental debris flows and the research on roll waves of clear water by [Cao et al. \(2015\)](#) demonstrated that the effects of turbulent stresses are considerable in water roll waves as large-scale vortexes arise behind the shocks. The $k - \varepsilon$ turbulence model is valid for fully developed, high-Reynolds-number clear water flows in the turbulent regime ([Rodi 1993](#)), which is not the case for debris flows. The high sediment concentration of debris flows may greatly affect the development of turbulence and trigger extremely complicated physical mechanisms that are still poorly understood. Generally, although the fluctuations of debris flows may differ from traditional turbulent motions, debris flows are far from laminar flows. Motivated by the work of [Cao et al. \(2015\)](#) in dealing with roll waves over steep slopes, the stresses due to fluctuations in the present model are therefore analogous to turbulent flows, and they are determined by the depth-averaged $k - \varepsilon$ turbulence model ([Rastogi and Rodi 1978](#)) and an empirical Reynolds stress-like modification component ([Ni 2010; Cao et al. 2015](#)) to show other impacts on turbulence motions.

$$T_R = T_0 + T_A \tag{24}$$

$$T_0 = -\rho \bar{U}'^2 = -\rho \left(2\nu_t \frac{\partial U}{\partial x} - \frac{2}{3}k \right) \tag{25a}$$

$$T_A = 2\alpha \rho h u_* \frac{\partial U}{\partial x} \tag{25b}$$

where k = depth-averaged fluctuation kinetic energy; $\nu_t = C_\mu k^2 / \varepsilon$ = depth-averaged eddy viscosity; ε = depth-averaged fluctuation dissipation rate; $u_* = \sqrt{\tau_b / \rho}$ = friction velocity; and α = empirical coefficient that is of great impact on debris flows modelling. According to

[Rastogi and Rodi \(1978\)](#), the depth-averaged $k - \varepsilon$ turbulence model is used here,

$$\frac{\partial(\rho h k)}{\partial t} + \frac{\partial(\rho h U k)}{\partial x} \tag{26}$$

$$= \frac{\partial}{\partial x} \left(\rho h \left(\frac{\nu_t}{\sigma_k} \right) \frac{\partial k}{\partial x} \right) + \rho h P_k + \rho h P_{kb} - \rho h \varepsilon$$

$$\frac{\partial(\rho h \varepsilon)}{\partial t} + \frac{\partial(\rho h U \varepsilon)}{\partial x} \tag{27}$$

$$= \frac{\partial}{\partial x} \left(\rho h \left(\frac{\nu_t}{\sigma_\varepsilon} \right) \frac{\partial \varepsilon}{\partial x} \right) + \rho h \frac{\varepsilon}{k} (C_{\varepsilon 1} P_k - C_{\varepsilon 2} \varepsilon) + \rho h P_{\varepsilon b}$$

$$P_k = 2\nu_t (\partial U / \partial x)^2 \tag{28a}$$

$$P_{kb} = C_f^{-1/2} (u_*)^3 / h \tag{28b}$$

$$P_{\varepsilon b} = C_r C_{\varepsilon 2} C_\mu^{1/2} C_f^{-3/4} u_*^4 / h^2 \tag{28c}$$

where P_k = the production terms from fluctuation due to the longitudinal velocity gradients; P_{kb} , $P_{\varepsilon b}$ = the production terms from non-uniformity of vertical profiles; and $C_f = \tau_b / \rho U^2$ = friction coefficient. The values of relevant empirical coefficients are listed in [Table 2](#).

Table 2 Coefficients in the depth-averaged $k - \varepsilon$ model

| Coefficient | C_μ | $C_{\varepsilon 1}$ | $C_{\varepsilon 2}$ | σ_k | σ_ε | C_r |
|-------------|---------|---------------------|---------------------|------------|----------------------|-------|
| Value | 0.09 | 1.44 | 1.92 | 1.0 | 1.3 | 3.6 |

Similarly, the depth-averaged viscous stress of debris flows can also be written as a relationship with depth-averaged kinematic viscosity ν_μ , which is approximately equal to the viscosity for fluid phase.

$$T_\mu = 2\rho \nu_\mu (\partial U / \partial x) \tag{29}$$

3 Numerical Algorithm

In order to facilitate mathematical manipulation, [Eqs. \(4\)-\(5\)](#) with primary variables z_b and f_{ak} are solved separately from [Eqs. \(1\)-\(3\)](#) and [Eqs. \(26\)-\(27\)](#) with primary variables h , U , c_k , k and ε , as [Eqs. \(4\)-\(5\)](#) are in essence ordinary differential equations. Yet all variables are updated at each time step.

The numerical algorithm employed in the present model is similar to [Xia et al. \(2017\)](#), which directly solve the original governing equations rather than first redistributing the water-sediment mixture density ([Cao et al. 2004; Wu and Wang 2008; Xia et al. 2010; Zhang and Duan 2011;](#)

Huang et al. 2014). Numerical fluxes are estimated by the well-balanced, WSDGM version of the SLIC scheme (Aureli et al. 2008). Detailed description and demonstration of the well-balanced property of the present model can be referred to Xia et al. (2017). Here, the numerical algorithm is just introduced simply. Firstly, Eqs.(1)-(3) and Eqs. (26)-(27) are written in a matrix form as

$$\frac{\partial \mathbf{U}}{\partial t} + \frac{\partial \mathbf{F}}{\partial x} = \mathbf{S}_b + \mathbf{S}_f + \mathbf{S}_d \quad (30)$$

$$\mathbf{U} = \begin{bmatrix} \rho h \\ \rho h U \\ \rho h c_k / \rho \\ \rho h k \\ \rho h \varepsilon \end{bmatrix} \quad \mathbf{F} = \begin{bmatrix} \rho h U \\ \rho h U^2 + \frac{1}{2} \frac{g_z}{\rho} (\rho h)^2 \\ \rho h U c_k / \rho \\ \rho h U k \\ \rho h U \varepsilon \end{bmatrix} \quad (31a, b)$$

$$\mathbf{S}_b = \begin{bmatrix} 0 \\ \rho h g_x - \rho h g_z \frac{\partial z_b}{\partial x} \\ 0 \\ 0 \\ 0 \end{bmatrix} \quad \mathbf{S}_f = \begin{bmatrix} \frac{\rho_0 (E-D)}{1-p} \\ -\tau_b \\ (E_k - D_k) \\ 0 \\ 0 \end{bmatrix} \quad (31c, d)$$

$$\mathbf{S}_d = \begin{bmatrix} 0 \\ \frac{\partial h (T_R + T_\mu)}{\partial x} \\ 0 \\ S_{dk} \\ S_{d\varepsilon} \end{bmatrix} \quad (31e)$$

$$S_{dk} = \frac{\partial}{\partial x} \left(\rho h \left(\frac{v_t}{\sigma_k} \right) \frac{\partial k}{\partial x} \right) + \rho h P_k + \rho h P_{kb} - \rho h \varepsilon \quad (31f)$$

$$S_{d\varepsilon} = \frac{\partial}{\partial x} \left(\rho h \left(\frac{v_t}{\sigma_\varepsilon} \right) \frac{\partial \varepsilon}{\partial x} \right) + \rho h \frac{\varepsilon}{k} (C_{\varepsilon 1} P_k - C_{\varepsilon 2} \varepsilon) + \rho h P_{\varepsilon b} \quad (31g)$$

where \mathbf{U} = conservative variables; \mathbf{F} = flux variables; \mathbf{S}_b = vector of gravitation and geometric terms; \mathbf{S}_f = vector of friction terms and effects from mass exchange with the bed; and \mathbf{S}_d = vector of other source terms including the stresses due to fluctuations, viscous stresses and the source terms in $k - \varepsilon$ model.

3.1 Finite volume discretization

An explicit finite volume discretization is employed along with a second-order Runge-Kutta method used for the source term \mathbf{S}_f and an implicit discretization method implemented for the source term \mathbf{S}_d

$$\mathbf{U}_i^p = \mathbf{U}_i^j - \frac{\Delta t}{\Delta x} (\mathbf{F}_{i+1/2}^j - \mathbf{F}_{i-1/2}^j) + \Delta t \mathbf{S}_{bi} \quad (32a)$$

$$\mathbf{U}_i^{pp} = \mathbf{U}_i^p + \Delta t \mathbf{S}_f^{RK} \quad (32b)$$

$$\mathbf{U}_i^{j+1} = \mathbf{U}_i^{pp} + \Delta t \mathbf{S}_d^{j+1} \quad (32c)$$

$$\mathbf{S}_f^{RK} = \frac{1}{2} [S_f(\mathbf{U}_i^p) + S_f(\mathbf{U}_i^{p*})] \quad (33a)$$

$$\mathbf{U}_i^{p*} = \mathbf{U}_i^p + \Delta t S_f(\mathbf{U}_i^p) \quad (33b)$$

where Δt = time step; Δx = spatial step; i = spatial node index; j = time node index; and $\mathbf{F}_{i+1/2}$ = inter-cell numerical flux at $x = x_{i+1/2}$ computed by a well-balanced version of second-order SLIC scheme (Aureli et al. 2008). To facilitate the well-balanced property on the inclined slope, the gravitation term is included in the \mathbf{S}_{bi} and the second component can be discretized as

$$\mathbf{S}_{bi} = \begin{cases} 0 \\ -\frac{[\bar{\mathbf{U}}_{i+1/2}^L(1) + \bar{\mathbf{U}}_{i-1/2}^R(1)]}{2} \left(g_x - g_z \frac{z_{bi+1/2} - z_{bi-1/2}}{\Delta x} \right) \\ 0 \\ 0 \\ 0 \end{cases} \quad (34)$$

where $\bar{\mathbf{U}}_{i+1/2}^L$ and $\bar{\mathbf{U}}_{i-1/2}^R$ = the reconstructed conservative variables; and $z_{bi+1/2} = (z_{bi+1} + z_{bi}) / 2$.

In Eq. (32c), the second-order terms in \mathbf{S}_d^{j+1} are discretized by

$$\frac{\partial}{\partial x} (M^{pp} \frac{\partial \psi}{\partial x}) \Big|_i^{j+1} = \frac{1}{\Delta x} \left(M_{i+1/2}^{pp} \frac{\partial \psi}{\partial x} \Big|_{i+1/2}^{j+1} - M_{i-1/2}^{pp} \frac{\partial \psi}{\partial x} \Big|_{i-1/2}^{j+1} \right) \quad (35)$$

where ψ = variables representing U , k and ε , and M = coefficient in line with ψ . The inter-cell values are calculated as linearized coefficients, i.e., $M_{i+1/2}^{pp} = (M_{i+1}^{pp} + M_i^{pp})/2$, $M_{i-1/2}^{pp} = (M_i^{pp} + M_{i-1}^{pp})/2$, and

$$(\partial \psi / \partial x)_{i+1/2}^{j+1} = (\psi_{i+1}^{j+1} - \psi_i^{j+1}) / \Delta x,$$

$$(\partial \psi / \partial x)_{i-1/2}^{j+1} = (\psi_i^{j+1} - \psi_{i-1}^{j+1}) / \Delta x.$$

As for the first-order term in \mathbf{S}_d^{j+1} related to k , it is discretized with a linearization of ρh as

$$\frac{\partial}{\partial x} \left(\frac{2}{3} \rho h k \right) \Big|_i^{j+1} = \frac{1}{3 \Delta x} \left[(\rho h)_{i+1}^{pp} k_{i+1}^{j+1} - (\rho h)_{i-1}^{pp} k_{i-1}^{j+1} \right] \quad (36)$$

The bed deformation and bed surface material composition are updated by the discretization of Eqs. (4) and (5) as follows

$$z_{bi}^{j+1} = z_{bi}^j + \Delta t \frac{(D_T - E_T)_i^{RK}}{1-p} \quad (37)$$

$$\frac{(\delta f_{ak})_i^{j+1} - (\delta f_{ak})_i^j}{\Delta t} + (f_{ik})_i^n \frac{\xi_i^{j+1} - \xi_i^j}{\Delta t} = \left(\frac{D_k - E_k}{1 - p} \right)_i^{RK} \quad (38)$$

Despite the stability of the implicit discretization method, the numerical scheme for the homogeneous hyperbolic system is explicit and the time step is specified according to the Courant-Friedrichs-Lewy (CFL) condition $\Delta t = C_r \Delta x / \lambda_{\max}$, where λ_{\max} = the maximum celerity computed from the Jacobian matrix $\partial F / \partial U$; and C_r = Courant number and a value of 0.95 is adopted in this paper.

3.2 Wet-dry front

The treatments of wet-dry interfaces are of great importance in numerical modelling and needs to be carefully handled in order to satisfy the well-balanced property of the numerical algorithm. Most well-balanced models are in the horizontal coordinate system or under the assumption of mild slopes, while the present model the is based on the inclined coordinate and takes the effects of bottom slope into consideration, which contributes to a different relationship derived from Eq. (2) that needs to be satisfied under stationary-flow cases ($U = 0$, $h = h_0 \neq 0$), i.e., $\partial \eta / \partial x = \tan \gamma$, where $\eta = h + z_b$ = water level. If the water level in a wet cell i is lower than the bed elevation of its adjacent dry cell $i + 1$ (i.e., $\eta_i + \Delta x \tan \gamma < z_{bi+1} = \eta_{i+1}$ in the inclined coordinate), then the water level of the dry cell and inter-cell bed elevation are both set to be the water level of the wet cell temporarily only when computing the numerical flux, which transfer to the present coordinate is $\eta_{i+1} = \eta_i + \Delta x \tan \gamma$ and $z_{bi+1/2} = \eta_i + \Delta x \tan \gamma / 2$. Similarly, if the water level in a wet cell $i + 1$ is lower than the bed elevation of its adjacent dry cell i (i.e., $\eta_{i+1} - \Delta x \tan \gamma < z_{bi} = \eta_i$ in the inclined coordinate), then $\eta_i = \eta_{i+1} - \Delta x \tan \gamma$ and $z_{bi+1/2} = \eta_{i+1} - \Delta x \tan \gamma / 2$ are obtained. It can be proved to satisfy the well-balanced property from mathematical derivation in the same way as Xia et al. (2017). The model is verified by cases of the irregular topography and the ideal dam-break flood to show its capabilities of preserving quiescent flow and dealing with wet-dry front on steep slopes, as can be seen in Supplementary (Appendix 2 and 3). Besides, to avoid the instabilities in numerical simulations due to the occurrence of very small water depth, the

computed water depth lower than the threshold depth (1×10^{-5} m) is set to be zero.

4 Model Comparison: USGS Debris Flows Experiments

Two categories of debris flow experiments are described in detail by Iverson et al. (2010) (fixed bed cases) and Iverson et al. (2011) (erodible bed cases). They recorded the unsteady, non-uniform debris flows from initiation to deposition at the USGS debris-flow flume. The measured flow-front velocity, flow thickness and bed deformation are used to compare the performance between the quasi single-phase model and the two-phase model (Li et al. 2017a, b), and to evaluate the influences of different closure models for bed shear stress on modelling debris flows.

The flume is a rectangular concrete channel 95 meters long, 2 meters wide, and 1.2 meters deep. Longitudinal distances in the flume are referenced to the 2-m high vertical headgate that is used to retain static debris prior to its release. Throughout most of its length, the flume bed slope is uniformly 31° , an angle typical of terrain where natural debris flows originate. At $x = 74$ m, the flume bed begins to flatten (Figure 1). The flow-front positions were tracked by playing videotapes frame by frame and recording the times at which the fronts reached reference stripes painted at 5-m intervals on the flume bed (Iverson et al. 2010). Measurements of flow thickness were made by laser flow-thickness sensors installed on crossbeams mounted above the bed at three cross sections, nominally located at $x = 32$ m, 66 m, and 90 m. Besides, the flow thickness at $x = 2$ m obtained by ultrasonic sensor was also presented. At the location $x = 13$ m, 23 m, 33 m and 43 m, erosion sensors were installed in the bed sediments, buried at depths of 2-10 cm, to detect the bed deformation (Figure 1b).

The subset of the fixed bed (FB) experiment (SGM rough bed, Iverson et al. 2010) and the subset of the erodible bed (EB) experiment (Experiment C $\theta = 0.25$, Iverson et al. 2011) are reproduced here. The initial debris flow was released by the sudden opening of the two-piece steel headgate. They moved across the smooth bed from $x = 0$ to 6 m with basal friction angle 28° and then the rough bed from $x = 6$ m with basal friction

angle 40°. Both of the debris in the FB and EB were composed of sand-gravel-mud (SGM) and the detailed grain-size distribution of the sediment mixture is given in Table 3. Although the two experiment subsets had some similar settings, each subset had different conditions. Specifically, in the EB, SGM mixture that covered the sloping flume bed from $x = 6$ m to 53 m was 12 cm thick, having volumetric water content $\theta = 0.25$ and sediment bed porosity $p = 0.48$, while the FB featured the bare concrete bed. 6 m³ of water-saturated sediment mixture was released from the headgate in EB, while approximately 10 m³ of mixture was used in the FB. Other detailed experimental elements for FB and EB are outlined in Table 4.

The present study focuses on the simulation of

Table 3 Grain-size distributions of SGM mixtures

| No. | d (mm) | Percent (%) | No. | d (mm) | Percent (%) |
|-----|----------|-------------|-----|----------|-------------|
| 1 | 0.0046 | 3.92 | 9 | 2.83 | 8.31 |
| 2 | 0.03 | 3.52 | 10 | 5.65 | 6.05 |
| 3 | 0.088 | 3.0 | 11 | 8.63 | 5.0 |
| 4 | 0.177 | 6.4 | 12 | 10.27 | 6.3 |
| 5 | 0.4 | 6.0 | 13 | 12.34 | 6.02 |
| 6 | 0.42 | 6.4 | 14 | 14.67 | 6.05 |
| 7 | 0.71 | 8.85 | 15 | 18.7 | 7.95 |
| 8 | 1.41 | 6.25 | 16 | 26.45 | 9.98 |

Note: SGM= Sand-gravel-mud.

Table 4 L^1 norm of the QSPE-RLM model with tuned α and U_w for fixed bed

| Values of the coefficients | α | | | U_w | | |
|----------------------------|----------|------|------|-------|------|------|
| | 1.12 | 1.6 | 2.08 | 3.5 | 5.0 | 6.5 |
| L^1 (%) | 3.48 | 2.56 | 3.12 | 8.43 | 2.56 | 3.37 |

the debris-flow evolution along the one-dimensional flume. Therefore, the computational domain includes the uniformly sloping flume and the adjacent runout pad that is assumed to have the same width as the flume. Some of the initial experimental conditions can be obtained from Table 4 and Figure 1, while the initial velocities and fluctuation kinetic energies and dissipation rates are set to be zero. The numerical simulations are performed within the time period before the forward and backward waves reach the downstream and upstream boundaries, thus the boundary conditions can be simply set according to the initial status.

The densities of fluid and solid phase are $\rho_f = 1100$ kg/m³ and $\rho_s = 2700$ kg/m³ (Iverson et al. 2010). In the CM, LM and RLM closure models, the Manning roughness n for smooth bed ($n_s = 0.012$) and rough bed ($n_r = 0.018$) are rectified using observed data from FB. In the BM model, coefficient $\bar{\mu} = 0.5$, $\chi = 0.6$, $\mu_s = 0$ in Eq. (13) are used following Berzi and Larcari (2013). In the LM closure models, $\mu_0 = 0.84$, $\mu_w = 0.11$, $U_w = 4$ m/s are suggested by Lucas et al. (2014). In the RLM closure models, $\mu_w = 0.11$, $U_w = 5$ m/s for FB and 2 m/s for EB respectively. The empirical coefficient $\alpha = 1.6$ in the modification term (Eq. (25b)) and the modification coefficient $\sigma = 2.0$ in Eq. (22) are determined by the measured thickness of FB at sections and the observed scour depth of EB respectively. The spatial step is set to be 0.05 m and CFL condition is satisfied.

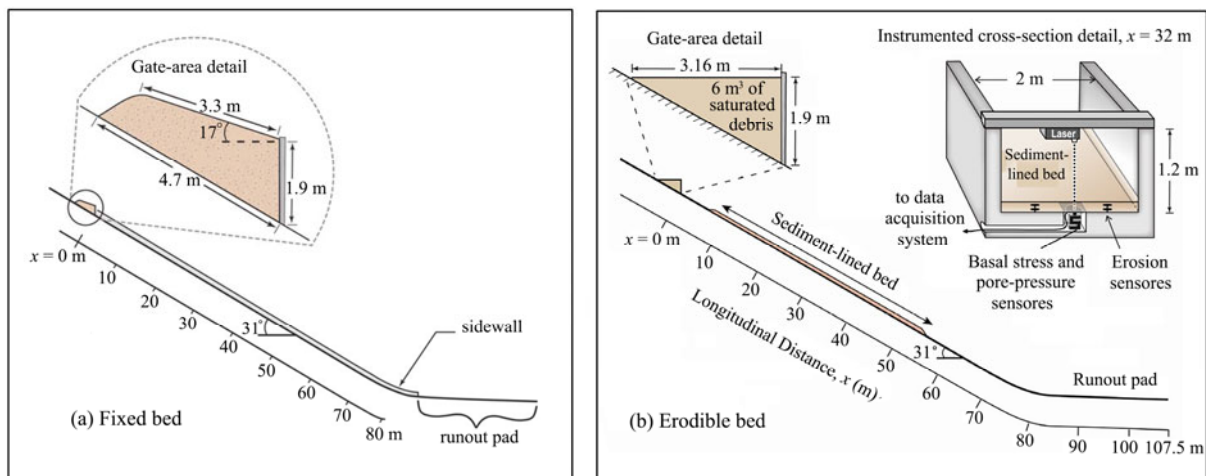


Figure 1 Schematic flume geometry of (a) fixed bed case and (b) erodible bed case along with instrumented cross section at $x = 32$ m (adapted from Iverson et al. 2010, 2011).

4.1 Fixed bed experiments

It is noted that in fixed bed cases, the sediment entrainment flux vanishes in governing equations because the bed was made of rigid material and was locally non-erodible. Figure 2 shows the computed flow front position of debris flows by QSPE model with four bed shear stress closure relationships of Table 1 and its comparison with simulations by the two-phase model (Li et al. 2017a) along with the measured data. It can be seen that the front advances faster than measure data using QSPE-BM model, and the deviations become farther with front propagation. The resistance formula derived analytically under steady and uniform conditions ignores the effects of the bed roughness. In contrast, the front positions computed by CM and LM models move much slower than the observed data, which demonstrates the predicted bed shear stresses are considerably overestimated. Despite the same resistance formula used by the QSPE-CM model and Li et al. (2017a), the different results from the two models are understandable. The latter one based on the two-phase flow theory incorporates interphase and particle-particle interaction forces and stresses due to the fluctuations of the solid motions, and it shows a good performance on front tracking. The parameters in the LM model is fitted by the landslide simulations of Lucas et al. (2014), thus may not be generally viable for the present debris flow case. However, according to Lucas et al. (2014), variations of the parameters are expected for each case individually. In the RLM model, the reasonable modification of the parameters leads to a better agreement between the results by the QSPE model and the measured.

Figure 3 illustrates the predicted flow thicknesses by the QSPE models (Table 1) compared with observed data, and the available computed results by Li et al. (2017a), George and Iverson (2014) and Ouyang et al. (2015) are also included in Figure 3. Apparently, simulations by Li et al. (2017a) agree with the experimental data best at all selected sections, showing its advantage of physically extended model. Results from QSPE-RLM model are also in good agreement with the observed by tuning the critical parameter U_w . Comparatively, models of George and Iverson (2014) and Ouyang et al. (2015) perform poorly. At

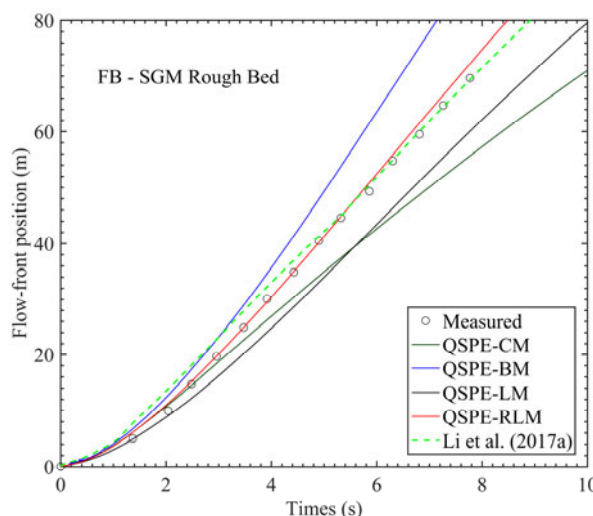


Figure 2 Flow front position of FB (Fixed Bed) computed by the QSPE-CM, QSPE-BM, QSPE-LM and QSPE-RLM models along with results from two-phase model by Li et al. (2017a) and measured data.

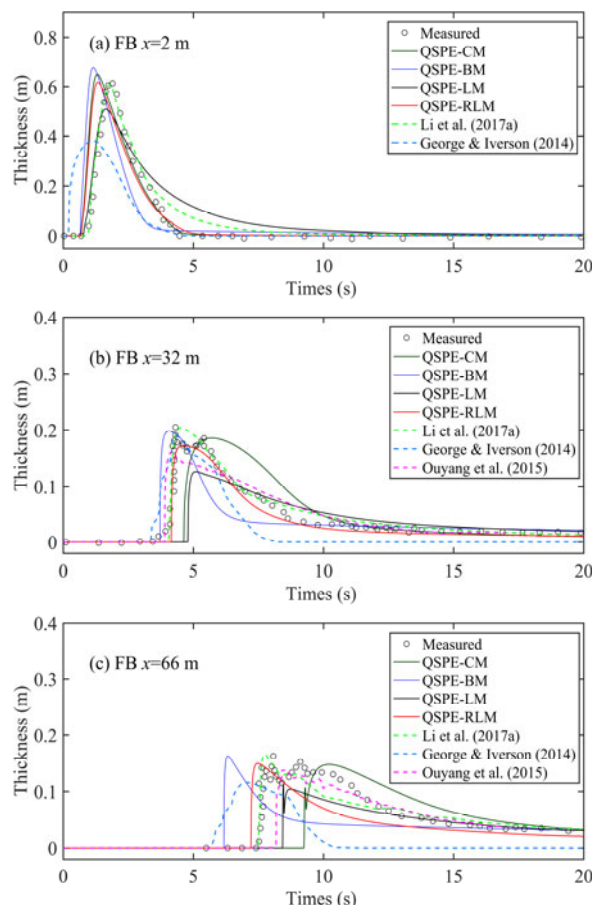


Figure 3 Flow thicknesses of FB (Fixed Bed) at selected sections computed by QSPE models, Li et al. (2017a), George and Iverson (2014) and Ouyang et al. (2015) along with measured data.

$x = 2$ m, the flow reaches at about $t = 0.8$ s, followed by a steep rising stage up to its peak of 0.6 m. But the flow front by George and Iverson (2014) reaches well ahead of the measured data and their peak values of the flow thicknesses are much lower than observed. Unfortunately, in Figure 3a ($x=2$ m) the results by Ouyang et al. (2015) are not available in their paper. The QSPE models with CM, BM and RLM perform similarly, showing a slightly differences in peak flow thickness, while the peak value decreases when LM relationship is used. The differences among the simulations by models enlarge gradually as the debris flow propagates (Figure 3 a-c), and become obvious at $x = 66$ m, where the underestimated shear stress by BM model causes the early front arrival and overestimated bed resistance predicted by CM and LM models leads to the late front arrival as compared to the measured. This is in accordance with the phenomenon present in Figure 2. It is also noted that although both CM and LM relationships are tend to overrate the bed shear stress, they have a different effect on the waveform. The LM model contributes to a flatter waveform than the CM model does.

4.2 Erodeable bed experiments

The bed erosion of a volume of 12 cm thick SGM mixture from $x = 6$ m to 53 m should be carefully considered in terms of the restrictive conditions, i.e., the non-erodeable constraint when bed elevation reaches the level of concrete flume bed.

Figure 4 compares the debris flow front propagation predicted by the QSPE models of Table 1 and Li et al. (2017b) with the measured data, and Figure 5 illustrates their computed flow thicknesses along with the results by Ouyang et al. (2015) at selected sections. The predictions of Ouyang et al. (2015) illustrate the advanced front arrival and lower peak thicknesses at selected sections as compared to the measured data. Similar to the results of front profiles for fixed bed, the overestimated bed shear stress by CM and LM closure models lead to the delayed computed fronts (Figure 4) and the flow thicknesses show the farther deviations from the observed (Figure 5). The QSPE-BM and QSPE-RLM models seem to have a good performance in tracking debris flow

front (Figure 4). However, the QSPE-BM model has difficulty in modelling the flow thickness at $x = 66$ m, showing a bimodal pattern of thicknesses, which is not the case as the measured data indicates (Figure 5). The QSPE-RLM model performs relatively better despite a slightly higher peak flow thickness at $x = 32$ m and a slightly lower peak thickness at $x = 66$ m. Comparatively, the simulations by Li et al. (2017b) agree best with the

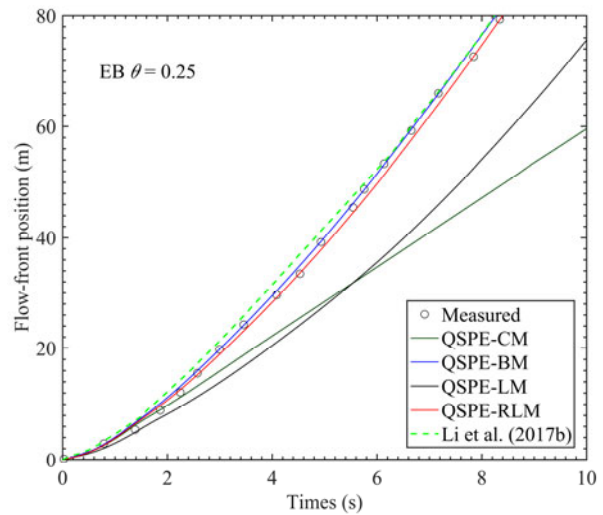


Figure 4 Flow front position of EB (Erodeable Bed) computed by the QSPE models with four closure relationships along with results from two-phase model by Li et al. (2017b) and measured data.

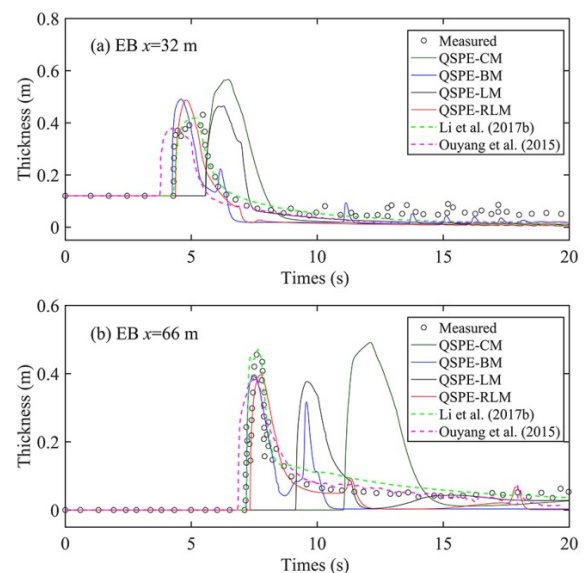


Figure 5 Flow thicknesses of EB (Erodeable Bed) at selected sections computed by QSPE models, Li et al. (2017b) and Ouyang et al. (2015) along with measured data.

measured data as compared to the other models. It demonstrates that two-phase formulation is superior for debris flow modelling as the relative motion and interphase interactions of the fluid and solid phases can be resolved.

Figure 6 shows the bed profiles from the QSPE-CM, QSPE-BM and QSPE-RLM models along with the measured data, and the simulations by Li et al. (2017b) are also included. The QSPE-CM model performs poorly compared to the measured, which indicates that the CM closure formula is not suitable for the QSPE model to simulate the debris flow. In comparison, the scouring speed computed by Li et al. (2017b) is in good agreement with the limited measured data, and the QSPE-BM and QSPE-RLM models also perform relatively well.

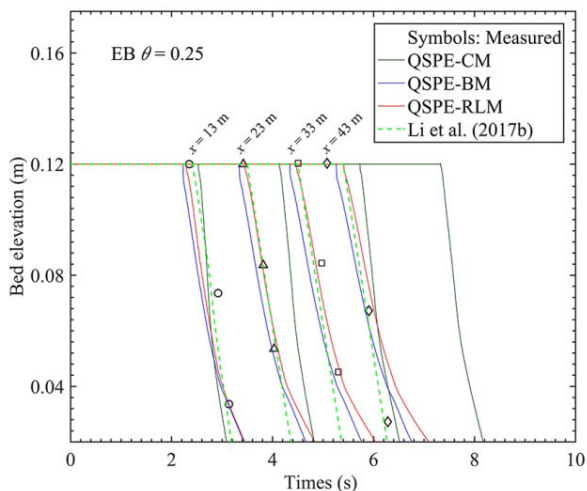


Figure 6 Temporal variations of EB (Erodible Bed) profiles computed by the QSPE-CM, QSPE-BM QSPE-RLM models and Li et al. (2017b) with measured data.

4.3 Discussion

Despite the superiority of the two-phase model (Li et al. 2017a, b) in its accuracy, the present QSPE model is still attractive as long as the proper bed shear stress relationship is chosen. The present QSPE model incorporates the effects of stresses due to fluctuations, which is believed to be crucial to the debris flow modelling. This subsection, using QSPE-RLM model in relation to FB test case, evaluates the effects of stresses due to fluctuations and assesses the sensitivities of the coefficients involved in the modification component of fluctuations stresses and the LM closure model.

Besides, the CPU runtime is compared between the two-phase model and the present QSPE-RLM model.

4.3.1 Effects of stresses due to fluctuations

The present QSPE-RLM model, the fluctuation stresses of which are incorporated and estimated by the depth-averaged turbulence model and a modification component, is compared with the QSPE-RLM model without T_R (noted as QSPE-RLM- $T_R=0$) or T_A (noted as QSPE-RLM- $T_A=0$) to demonstrate the effects of T_R , T_0 and T_A (Eq. (24)) on modelling. Figures 7 and 8 show the computed front positions and flow thicknesses at selected sections from QSPE-RLM models without T_R or T_A , compared with those from complete QSPE-RLM model and the measured. It can be seen that involving the stresses due to fluctuations greatly improves the performance in modelling debris flows. It is found that the fluctuation stresses modelled only by $k-\epsilon$ turbulence model (i.e., QSPE-RLM- $T_A=0$) leads to slightly decrease in the peak thicknesses at sections (Figure 8), while adding modification component increases the peak thicknesses, which consequently improves the model performance, especially at $x = 2$ m (Figure 8a). From a physical perspective, this is justified because the stress term due to fluctuation S_{TR} ($S_{TR} = \partial \rho h T_R / \partial x$) in the momentum conservation Eq. (2) is by no means negligible compared with

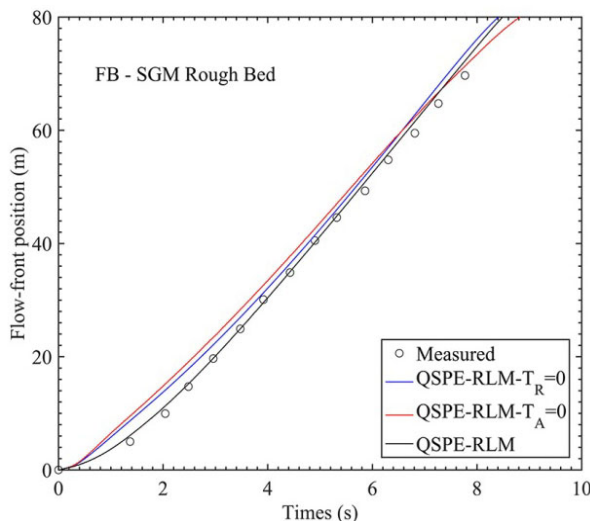


Figure 7 Flow front position of FB (Fixed Bed) computed by the QSPE-RLM model without T_R or T_A , compared with complete QSPE-RLM model and measured data.

the gravitational term $S_G = \rho hg \sin \gamma$. This effect is similar to that of the longitudinal gradient of normal turbulent stress on roll waves in shallow clear-water flows on steep slopes (Cao et al. 2015). It is also indicated that the additional modification component mainly affects the beginning of debris flow evolution ($t \leq 4$ s in Figure 7 and $x = 2$ m in Figure 8a). It is critical to flag out that the appearance of oscillations exists in the computed results by the QSPE-RLM model without T_R or T_A , which however may not be construed as physically reasonable. The stresses due to fluctuations are physically existed and considerable (Iverson et al. 2010; Cao et al. 2015) and can be derived mathematically by time-averaging the original full three dimensional momentum conservation equations. The high sediment concentration of debris flows may greatly affect the development of turbulence, thus only using $k-\varepsilon$ turbulence

model is not suitable to close the fluctuation stresses as it is valid for fully developed, high-Reynolds-number clear water flows in the turbulent regime (Rodi 1993). In order to provide insight into the contributions of the stresses due to fluctuations consisting of T_0 and T_A in Eq. (24), the spatial distribution ratios of S_{T_0}/S_G ($S_{T_0} = \partial \rho h T_0 / \partial x$) and S_{T_A}/S_G ($S_{T_A} = \partial \rho h T_A / \partial x$) at specific instants from QSPE-RLM model are present in relation to FB, as shown in Figure 9. In accordance with the previous computed results, both S_{T_0} and S_{T_A} have great effects on the early stage of debris flows (Figure 9a), the modification component term S_{T_A} which is negative and contrary to S_{T_0} . Compared to the gravitational term S_G , after $t = 2$ s, the values of S_{T_0} and S_{T_A} are negligible from the trough to the peak of the debris flow, whereas both are considerable around the debris flow front (Figure 9 b, c).

4.3.2 Sensitivity analysis

It is interesting to evaluate the sensitivity of the simulations of present complete QSPE-RLM model to coefficients α involved in the modification component of stresses due to fluctuations (Eq. (24)) and the coefficient U_w in RLM closure relationship (Eq. (17)). Thus in the QSPE-RLM model, α and U_w are tuned by 30% in relation to FB, and L^1 norm of flow front location is deployed to quantify their impacts on debris flow modelling, which is defined as $L^1 = \sum |x_f - x_f^*| / \sum x_f^* \times 100\%$, where x_f = computed flow front location; x_f^* = measured flow front location. Figure 10 compares the computed flow front positions using different α and U_w by the QSPE-RLM model for FB. Interestingly, α mainly affects the first half of the debris flow (Figure 10a), while U_w has an impact mostly on the latter part (Figure 10b). Echoing Figure 10, a larger α leads to a relative slower front speed, but the changes decreased with time and its effects are almost negligible after about $t = 6$ s. While the decreased U_w contributes to the smaller bed resistance and accordingly, flow front propagates faster. The values of L^1 norm in relation to the tuned values of α and U_w in Table 4 provide quantitative insight into their effects on flow front location. They are appreciable but limited. And it also suggests that the simulation with the calibrated α and U_w agree well with the measured data in FB.

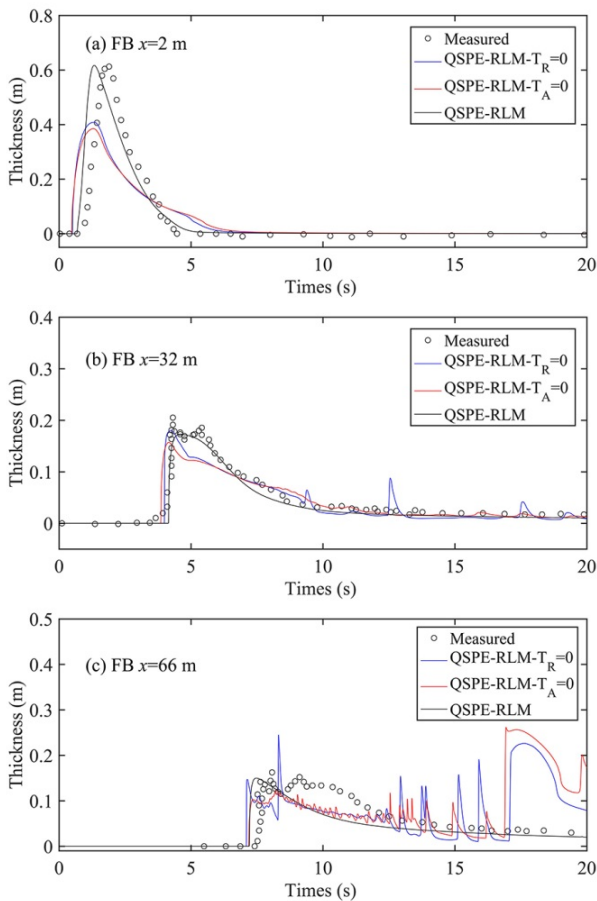


Figure 8 Flow thicknesses of FB (Fixed Bed) at selected sections computed by the QSPE-RLM model without T_R or T_A , compared with complete QSPE-RLM model and measured data.

4.3.3 CPU runtime

In order to compare the computational cost of the present complete QSPE model and the two-phase model by Li et al. (2017a, b), the CPU runtime of the two kinds of models for FB and EB cases relative to that of the QSPE-RLM model for FB are listed in Table 5. It indicates that the erodible bed case takes more CPU time than fixed bed case as the former involves the bed evolution equation which shows the mass exchange between the flow and the bed. The CPU time of two-phase model is approximately 22% for FB and 25% for EB longer than that of quasi single-phase mixture model, which is mainly affected by the number of the size groups of the solid phases. For N size sediment classes, the two-phase model (Eqs. (1), (6-8), (4-5)) have additional N momentum conservation equations for size-specific solid phases as compared to its counterpart (Eqs. (1-5)). Besides, to closure these size-specific momentum equations, $2N$ equations for solving the solid fluctuation are introduced (Li et al. 2017a, b). Thus, it is predicable that the CPU runtime of the two-phase model increases inevitably, especially in natural large-scale debris flows that characterized by a broad particle size distribution.

5 Conclusions

Based on the shallow water hydro-sediment-morphodynamic theory, a depth-averaged quasi single-phase mixture model is proposed for debris flows. A fully conservative numerical algorithm with well-balanced slope limited centred scheme is used to solve the governing equations. Appropriate bed stresses estimation of RLM model plays a central role in accurately reproducing debris flows. The complete QSPE-RLM model has superiority over the traditional QSPE models of George and Iverson

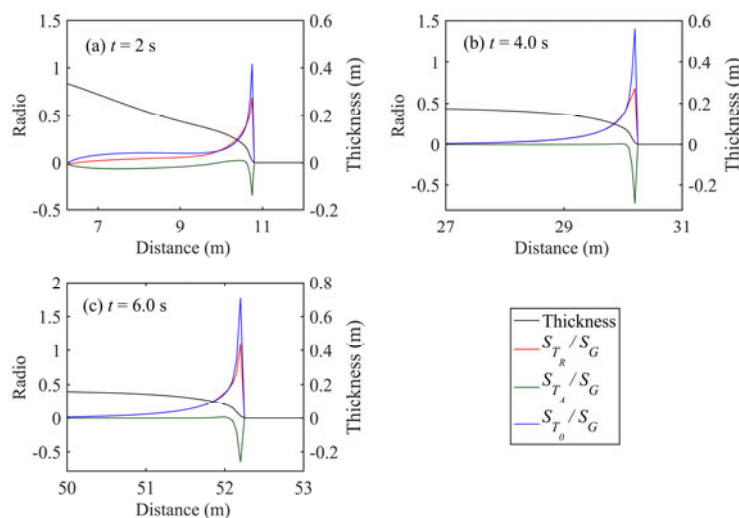


Figure 9 The ratios of stress terms due to fluctuations to the gravitational term along with the flow thicknesses at several instants computed by QSPE-RLM model in relation to of FB (Fixed Bed).

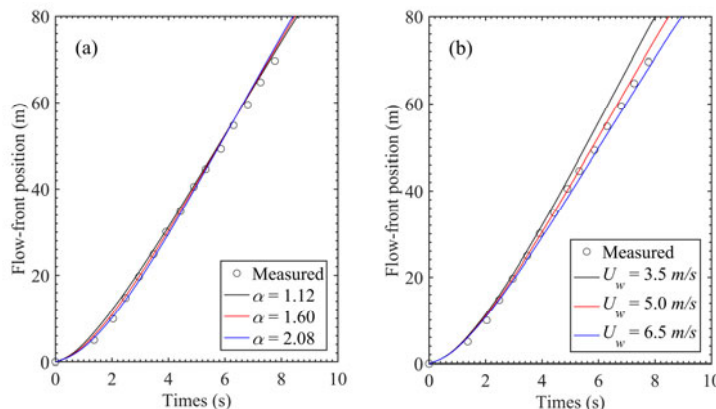


Figure 10 Sensitivities of the computed flow front positions by QSPE-RLM model to coefficients α and U_w in relation to of FB (Fixed Bed).

Table 5 Relative CPU runtime of QSPE-RLM model and the two-phase model by Li et al. (2017a, b)

| Model | FB SGM Rough Bed | EB $\theta = 0.25$ |
|-------------------------------------|------------------|--------------------|
| QSPE-LMR | 1.0 | 1.05 |
| Two-phase model (Li et al. 2017a,b) | 1.22 | 1.31 |

Notes: FB=Fixed Bed; EB=Erodible Bed.

(2014) and Ouyang et al. (2015). It facilitates a step forward in debris flow modelling under the framework of quasi single-phase mixture flow theory for its inclusion of the stresses due to fluctuations. Although the two-phase model by Li et al. (2017a, b) performs relatively better than the present QSPE model, the QSPE model is still attractive as the CPU runtime of the two-phase model increases inevitably with the number of the size groups of the solid phases.

Further studies are necessary to delimit the uncertainty from the estimations of bed resistances, mass exchange with the bed as well as the closure models for stresses due to fluctuations. Interphase and particle-particle interactions remain unresolved by the present QSPE model, which characterizes the need for physically enhanced two-phase models. Meanwhile, in order to apply the model to natural debris flows, extension to two dimensions is also warranted in future research.

References

- Ancey C (2001) Debris flows and related phenomena. In: Balmforth NJ and Provenzale A (eds.), *Geomorphological Fluid Mechanics*. Springer, Heidelberg Germany. pp 528-547.
- Armanini A, Capart H, Fraccarollo L, et al. (2005) Rheological stratification in experimental free-surface flows of granular-liquid mixtures. *Journal of Fluid Mechanics* 532: 269-319. <https://doi.org/10.1017/S0022112005004283>
- Armanini A, Fraccarollo L, Rosatti G (2009) Two-dimensional simulation of debris flows in erodible channels. *Computers & Geosciences* 35(5): 993-1006. <https://doi.org/10.1016/j.cageo.2007.11.008>
- Aureli F, Maranzoni A, Mignosa P, et al. (2008) A weighted surface-depth gradient method for the numerical integration of the 2D shallow water equations with topography. *Advances in Water Resources* 31(7): 962-974. <https://doi.org/10.1016/j.advwatres.2008.03.005>
- Balmforth NJ, Liu JJ (2004) Roll waves in mud. *Journal of Fluid Mechanics* 519: 33-54. <https://doi.org/10.1017/S0022112004000801>
- Beeler NM, Tullis TE, Goldsby DL (2008) Constitutive relationships and physical basis of fault strength due to flash heating. *Journal of Geophysical Research - Solid Earth* 113(B1): B01401. <https://doi.org/10.1029/2007JB004988>
- Berti M, Genevois R, Simoni A, et al. (1999) Field observations of a debris flow event in the Dolomites. *Geomorphology* 29(3-4): 265-274. [https://doi.org/10.1016/S0169-555X\(99\)00018-5](https://doi.org/10.1016/S0169-555X(99)00018-5)
- Berzi D, Jenkins JT (2008) A theoretical analysis of free-surface flows of saturated granular-liquid mixtures. *Journal of Fluid Mechanics* 608: 393-410. <https://doi.org/10.1017/S0022112008002401>
- Berzi D, Larcan E (2013) Flow resistance of inertial debris flows. *Journal of Hydraulic Engineering* 139(2): 187-194. [https://doi.org/10.1061/\(asce\)hy.1943-7900.0000664](https://doi.org/10.1061/(asce)hy.1943-7900.0000664)
- Berger C, McArdell BW, Schlunegger F (2011) Direct measurement of channel erosion by debris flows, Illgraben, Switzerland. *Journal of Geophysical Research- Earth Surface* 116(F1): F01002. <https://doi.org/10.1029/2010jfo01722>
- Bouchut F, Fernandez-Nieto ED, Mangeney A, et al. (2015) A two-phase shallow debris flow model with energy balance. *ESAIM-Mathematical Modelling and Numerical Analysis-modélisation Mathématique ET Analyse Numérique* 49(1): 101-140. <https://doi.org/10.1051/m2an/2014026>
- Brufau P, Garcia-Navarro P, Ghilardi P, et al. (2000) 1D mathematical modelling of debris flow. *Journal of Hydraulic Research* 38(6): 435-446. <https://doi.org/10.1080/00221680009498297>
- Cao Z, Pender G, Wallis S, et al. (2004) Computational dam-break hydraulics over erodible sediment bed. *Journal of Hydraulic Engineering* 130(7): 689-703. [https://doi.org/10.1061/\(ASCE\)0733-9429\(2004\)130:7\(689\)](https://doi.org/10.1061/(ASCE)0733-9429(2004)130:7(689))
- Cao Z, Li Z, Pender G, et al. (2012) Non-capacity or capacity model for fluvial sediment transport. *Proceedings of the Institution of Civil Engineers - Water Management* 165(4): 193-211. <https://doi.org/10.1680/wama.10.00035>
- Cao Z, Hu P, Hu K, et al. (2015) Modeling roll waves with shallow water equations and turbulent closure. *Journal of Hydraulic Research* 53(2): 161-177. <https://doi.org/10.1080/00221686.2014.950350>
- Cao Z, Hu P, Pender G, et al. (2016) Non-capacity transport of non-uniform bed load sediment in alluvial rivers. *Journal of Mountain Science* 13(3): 377-396. <https://doi.org/10.1007/s11629-015-3710-8>
- Cao Z, Xia C, Pender G, et al. (2017) Shallow water hydro-sediment-morphodynamic equations for fluvial processes. *Journal of Hydraulic Engineering* 143(5): 02517001. [https://doi.org/10.1061/\(ASCE\)HY.1943-7900.0001281](https://doi.org/10.1061/(ASCE)HY.1943-7900.0001281)
- Cardoso-Landa G (2009) Associated disasters to the debris flows. In: Starrett S (ed.), *Proceedings of the 2009 World Environmental and Water Resources Congress, Kansas City, Missouri, USA*. pp 5833-5844. [https://doi.org/10.1061/41036\(342\)590](https://doi.org/10.1061/41036(342)590)
- Cascini L, Cuomo S, Pastor M, et al. (2008) Geomechanical modelling of triggering mechanisms for rainfall-induced triangular shallow landslides of the flow type. In: Sanchez-Marre M, Bejar J, Comas J, et al. (eds), *International Environmental Modelling and Software Society (iEMSs), Manno*. pp 1516-1523.
- Cascini L, Cuomo S, Pastor M (2013) Inception of debris avalanches: remarks on geomechanical modelling. *Landslides* 10(6): 701-711. <https://doi.org/10.1007/s10346-012-0366-0>
- Chiang SH, Chang KT, Mondini AC, et al. (2012) Simulation of event-based landslides and debris flows at watershed level. *Geomorphology* 138: 306-318. <https://doi.org/10.1016/j.geomorph.2011.09.016>
- Cozzolino L, Cimorelli L, Covelli C, et al. (2014) A novel numerical approach for 1D variable density shallow flows over uneven rigid and erodible beds. *Journal of Hydraulic Engineering* 140(3): 254-268. [https://doi.org/10.1061/\(asce\)hy.1943-7900.0000821](https://doi.org/10.1061/(asce)hy.1943-7900.0000821)
- Coussot P, Meunier M (1996) Recognition, classification and mechanical description of debris flows. *Earth-Science Reviews* 40(3-4): 209-227. [https://doi.org/10.1016/0012-8252\(95\)00065-8](https://doi.org/10.1016/0012-8252(95)00065-8)
- Cui YT, Paola C, Parker G (1996) Numerical simulation of aggradation and downstream fining. *Journal of Hydraulic Research* 34(2): 185-204. <https://doi.org/10.1080/00221689609498496>
- Cui P, Zhou GGD, Zhu XH, et al. (2013) Scale amplification of natural debris flows caused by cascading landslide dam failures. *Geomorphology* 182: 173-189. <https://doi.org/10.1016/j.geomorph.2012.11.009>
- D'Aniello A, Cozzolino L, Cimorelli L, et al. (2015) A numerical model for the simulation of debris flow triggering, propagation and arrest. *Natural Hazards* 75(2): 1403-1433. <https://doi.org/10.1007/s11069-014-1389-8>
- Denlinger RP, Iverson RM (2001) Flow of variably fluidized granular masses across three-dimensional terrain: 2. Numerical predictions and experimental tests. *Journal of*

Acknowledgments

The work reported in this manuscript is funded by Natural Science Foundation of China (Grants Nos. 51279144 and 11432015).

Electronic supplementary material: Supplementary materials (Appendixes 1-3) are available in the online version of this article at <https://doi.org/10.1007/s11629-018-4886-5>.

- Geophysical Research - Solid Earth 106(B1): 553-566. <https://doi.org/10.1029/2000jb900330>
- Di Silvio G, Gregoretti C (1997) Gradually varied debris flow along a slope. In: Chen CL (ed), Debris-Flow Hazards Mitigation: Mechanics, Prediction & Assessment, San Francisco, California, USA. pp 767-776.
- Di Cristo C, Iervolino M, Vacca A (2014) Applicability of Kinematic, Diffusion and Quasi-Steady dynamic wave models to shallow mud flows. *Journal of Hydrologic Engineering*, 19(5): 956-965. [https://doi.org/10.1061/\(asce\)he.1943-5584.0000881](https://doi.org/10.1061/(asce)he.1943-5584.0000881)
- Di Cristo C, Iervolino M, Vacca A (2015) On the stability of gradually-varying mud flows in open channels. *Meccanica* 50(4): 963-979. <https://doi.org/10.1007/s11012-014-0075-y>
- Di Cristo C, Greco M, Iervolino M, et al. (2016) Two-dimensional two-phase depth-integrated model for transients over mobile bed. *Journal of Hydraulic Engineering* 142(2): 04015043. [https://doi.org/10.1061/\(asce\)hy.1943-7900.0001024](https://doi.org/10.1061/(asce)hy.1943-7900.0001024)
- Di Cristo C, Iervolino M, Vacca A (2018) Applicability of Kinematic and Diffusive models for mud-flows: a steady state analysis. *Journal of Hydrology* 559: 585-595. <https://doi.org/10.1016/j.jhydrol.2018.02.016>
- Egashira S (2011) Prospects of debris flow studies from constitutive relations to governing equations. *Journal of Disaster Research* 6(3): 313-320. <https://doi.org/10.20965/jdr.2011.p0313>.
- George DL, Iverson RM (2014) A depth-averaged debris-flow model that includes the effects of evolving dilatancy. II. Numerical predictions and experimental tests. *Proceedings of the Royal Society A - Mathematical Physical and Engineering Sciences* 470(2170): 20130820. <https://doi.org/10.1098/rspa.2013.0820>
- Gray JMNT, Wieland M, Hutter K (1999) Gravity-driven free surface flow of granular avalanches over complex basal topography. *Proceedings of the Royal Society A - Mathematical Physical and Engineering Sciences* 455(1985): 1841-1874. <https://doi.org/10.1098/rspa.1999.0383>
- Greco M, Iervolino M, Leopardi A, et al. (2012) A two-phase model for fast geomorphic shallow flows. *International Journal of Sediment Research* 27(4): 409-425. [https://doi.org/10.1016/s1001-6279\(13\)60001-3](https://doi.org/10.1016/s1001-6279(13)60001-3)
- Gregoretti C, Degetto M, Boreggio M (2016) GIS-based cell model for simulating debris flow runout on a fan. *Journal of Hydrology* 534: 326-340. <https://doi.org/10.1016/j.jhydrol.2015.12.054>
- Guadagno FM, Forte R, Revellino P, et al. (2005) Some aspects of the initiation of debris avalanches in the Campania Region: the role of morphological slope discontinuities and the development of failure. *Geomorphology* 66: 237-254. <https://doi.org/10.1016/j.geomorph.2004.09.024>
- Hirano M (1971) River bed degradation with armouring. *Proceedings of Japan Society of Civil Engineers, Tokyo, Japan*. pp 55-65. (In Japanese)
- Hoey TB, Ferguson R (1994) Numerical simulation of downstream fining by selective transport in gravel bed rivers: Model development and illustration. *Water Resources Research* 30(7): 2251-2260. <https://doi.org/10.1029/94wr00556>
- Hotta N, Tsunetaka H, Suzuki T (2015) Interaction between topographic conditions and entrainment rate in numerical simulations of debris flow. *Journal of Mountain Science* 12(6): 1383-1394. <https://doi.org/10.1007/s11629-014-3352-2>
- Hu K, Pu L, Wang X (2016) Experimental study of entrainment behavior of debris flow over channel inflexion points. *Journal of Mountain Science* 13(6): 971-984. <https://doi.org/10.1007/s11629-015-3749-6>
- Huang W, Cao Z, Carling P, et al. (2014) Coupled 2D hydrodynamic and sediment transport modeling of megaflood due to glacier dam-break in Altai Mountains, Southern Siberia. *Journal of Mountain Science* 11(6): 1442-1453. <https://doi.org/10.1007/s11629-014-3032-2>
- Hunt B (1994) Newtonian Fluid Mechanics Treatment of Debris Flows and Avalanches. *Journal of Hydraulic Engineering* 120(12): 1350-1363. [https://doi.org/10.1061/\(asce\)0733-9429\(1994\)120:12\(1350\)](https://doi.org/10.1061/(asce)0733-9429(1994)120:12(1350))
- Hutter K, Svendsen B, Rickenmann D (1994) Debris flow modeling: A review. *Continuum Mechanics and Thermodynamics* 8(1): 1-35. <https://doi.org/10.1007/s001610050026>
- Hürlimann M, Rickenmann D, Graf C (2003) Field and monitoring data of debris-flow events in the Swiss Alps. *Canadian Geotechnical Journal* 40(1): 161-175. <https://doi.org/10.1139/t02-087>
- Hürlimann M, McArdell BW, Rickli C (2015) Field and laboratory analysis of the runout characteristics of hillslope debris flows in Switzerland. *Geomorphology* 232: 20-32. <https://doi.org/10.1016/j.geomorph.2014.11.030>
- Imaizumi F, Tsuchiya S, Ohsaka O (2016) Field observations of debris-flow initiation processes on sediment deposits in a previous deep-seated landslide site. *Journal of Mountain Science* 13(2): 213-222. <https://doi.org/10.1007/s11629-015-3345-9>
- Imran J, Parker G, Locat J, et al. (2001) 1D numerical model of muddy subaqueous and subaerial debris flows. *Journal of Hydraulic Engineering* 127(11): 959-968. [https://doi.org/10.1061/\(asce\)0733-9429\(2001\)127:11\(959\)](https://doi.org/10.1061/(asce)0733-9429(2001)127:11(959))
- Iverson RM (1997) The physics of debris flows. *Reviews of Geophysics* 35(3): 245-296. <https://doi.org/10.1029/97rg00426>
- Iverson RM (2000) Landslide triggering by rain infiltration. *Water Resources Research* 36(7):1897-1910. <https://doi.org/10.1029/2000wr900090>
- Iverson RM, Logan M, LaHusen RG, et al. (2010) The perfect debris flow? Aggregated results from 28 large-scale experiments. *Journal of Geophysical Research - Earth Surface* 115(F3): F03005. <https://doi.org/10.1029/2009jfo01514>
- Iverson RM, Reid ME, Logan M, et al. (2011) Positive feedback and momentum growth during debris-flow entrainment of wet bed sediment. *Nature Geoscience* 4: 116-121. <https://doi.org/10.1038/ngeo1040>
- Jeng CJ, Sue DZ (2016) Characteristics of ground motion and threshold values for colluvium slope displacement induced by heavy rainfall: a case study in northern Taiwan. *Natural Hazards and Earth System Sciences* 16(6):1309-1321. <https://doi.org/10.5194/nhess-16-1309-2016>
- Laigle D, Coussot P (1997) Numerical modeling of mudflows. *Journal of Hydraulic Engineering* 123(7): 617-623. [https://doi.org/10.1061/\(asce\)0733-9429\(1997\)123:7\(617\)](https://doi.org/10.1061/(asce)0733-9429(1997)123:7(617))
- Li J, Cao Z, Hu K, et al. (2017a) A depth-averaged two-phase model for debris flows over fixed beds. *International Journal of Sediment Research*, in press. <https://doi.org/10.1016/j.ijsrc.2017.06.003>
- Li J, Cao Z, Hu K, et al. (2017b) A depth-averaged two-phase model for debris flows over erodible beds. *Earth Surface Processes and Landforms* 43(4): 817-839. <https://doi.org/10.1002/esp.4283>
- Liu K, Huang M (2006) Numerical simulation of debris flow with application on hazard area mapping. *Computational Geosciences* 10(2): 221-240. <https://doi.org/10.1007/s10596-005-9020-4>
- Luca L, Hutter K, Kuo CY, et al. (2009) Two-layer models for shallow avalanche flows over arbitrary variable topography. *International Journal of Advances in Engineering Sciences and Applied Mathematics* 1(2-3): 99-121. <https://doi.org/10.1007/s12572-010-0006-7>
- Lucas A, Mangeney A, Ampuero JP (2014) Frictional velocity-weakening in landslides on Earth and on other planetary bodies. *Nature Communications* 2014 5:417. <https://doi.org/10.1038/ncomms4417>
- Mangeney A, Roche O, Hungr O, et al. (2010) Erosion and mobility in granular collapse over sloping beds. *Journal of Geophysical Research- Earth Surface* 115(F3): F03040. <https://doi.org/10.1029/2009jfo01462>
- McArdell BW, Bartelt P, Kowalski J (2007) Field observations of basal forces and fluid pore pressure in a debris flow. *Geophysical Research Letters* 34(7): L07406. <https://doi.org/10.1029/2006gl029183>
- Meng X, Wang Y (2016) Modelling and numerical simulation of two-phase debris flows. *Acta Geotechnica* 11(5): 1027-1045. <https://doi.org/10.1007/s11440-015-0418-4>
- Meng X, Wang Y, Wang C, et al. (2017) Modeling of unsaturated

- granular flows by a two-layer approach. *Acta Geotechnica* 12(3): 677-701. <https://doi.org/10.1007/s11440-016-0509-x>
- Ni H (2010) Turbulence simulation and application in modern hydraulics engineering. China Water Power Press, Beijing. (In Chinese)
- O'Brien JS (1986) Physical processes, rheology and modeling of mudflows. PhD thesis, Colorado State University.
- Okuda S, Suwa H, Okunishi K, et al. (1977) Synthetic observation on debris flow, Part 3. Observation at valley Kamikamihorizawa of Mt. Yakedake in 1976. *Annals of Disaster Prevention Research Institute, Kyoto University* 20B-1: 237-263. (In Japanese)
- Ouyang C, He S, Tang C (2015) Numerical analysis of dynamics of debris flow over erodible beds in Wenchuan earthquake-induced area. *Engineering Geology* 194: 62-72. <https://doi.org/10.1016/j.enggeo.2014.07.012>
- Pailha M, Pouliquen O (2009) A two-phase flow description of the initiation of underwater granular avalanches. *Journal of Fluid Mechanics* 633: 115-135. <https://doi.org/10.1017/S0022112009007460>
- Parker G (1991) Selective sorting and abrasion of river gravel. I: Theory. *Journal of Hydraulic Engineering* 117(2): 131-149. [https://doi.org/10.1061/\(asce\)0733-9429\(1991\)117:2\(131\)](https://doi.org/10.1061/(asce)0733-9429(1991)117:2(131))
- Parsons JD, Whipple KX, Simoni A (2001) Experimental Study of the Grain-Flow, Fluid-Mud Transition in Debris Flows. *Journal of Geology* 109(4): 427-447. <https://doi.org/10.1086/320798>
- Pelanti M, Bouchut F, Mangeney A (2008) A Roe-Type scheme for two-phase shallow granular flows over variable topography. *ESAIM-Mathematical Modelling and Numerical Analysis-modelisation Mathematique ET Analyse Numerique* 42(5): 851-885. <https://doi.org/10.1051/m2an:2008029>
- Pitman EB, Le L (2005) A two-fluid model for avalanche and debris flows. *Philosophical Transactions of the Royal Society A-Mathematical Physical and Engineering Sciences* 363(1832): 1573-1601. <https://doi.org/10.1098/rsta.2005.1596>
- Pudasaini SP, Wang Y, Hutter K (2005) Modelling debris flows down general channels. *Natural Hazards and Earth System Science* 5(6): 799-819. <https://doi.org/10.5194/nhess-5-799-2005>
- Pudasaini SP (2012) A general two-phase debris flow model. *Journal of Geophysical Research- Earth Surface* 117(F3): F03010. <https://doi.org/10.1029/2011JF002186>
- Rastogi AK, Rodi W (1978) Predictions of heat and mass transfer in open channels. *Journal of the Hydraulics Division* 104(3): 397-420.
- Rengers FK, McGuire LA, Kean JW, et al. (2016) Model simulations of flood and debris flow timing in steep catchments after wildfire. *Water Resources Research* 52(8): 6041-6061. <https://doi.org/10.1002/2015WR018176>
- Rice RJ (2006) Heating and weakening of faults during earthquake slip. *Journal of Geophysical Research - Solid Earth* 111(B5): B05311. <https://doi.org/10.1029/2005JB004006>
- Richardson JF, Zaki WN (1954) Sedimentation and fluidisation: Part 1. *Chemical Engineering Research and Design* 75: s82-s99. [https://doi.org/10.1016/S0263-8762\(97\)80006-8](https://doi.org/10.1016/S0263-8762(97)80006-8)
- Rickenmann D, Zimmermann M (1993) The 1987 debris flows in Switzerland: documentation and analysis. *Geomorphology* 8(2-3): 175-189. [https://doi.org/10.1016/0169-555X\(93\)90036-2](https://doi.org/10.1016/0169-555X(93)90036-2)
- Rosatti G, Begnudelli L (2013) Two-dimensional simulation of debris flows over mobile bed: Enhancing the TRENT2D model by using a well-balanced Generalized Roe-type solver. *Computers & Fluids* 71: 179-195. <https://doi.org/10.1016/j.compfluid.2012.10.006>
- Rodi W (1993) Turbulence models and their applications in Hydraulics- a State of the Art Review, 3rd edn. IAHR Monograph, Balkema, Rotterdam, The Netherlands.
- Santi PM, de Wolfe VG, Higgins JD, et al. (2008) Sources of debris flow material in burned areas. *Geomorphology* 96(3-4): 310-321. <https://doi.org/10.1016/j.geomorph.2007.02.022>
- Sarno L, Carravetta A, Martino R, et al. (2013) Pressure coefficient in dam-break flows of dry granular matter. *Journal of Hydraulic Engineering* 139 (11): 1126-1133. [https://doi.org/10.1061/\(ASCE\)HY.1943-7900.0000772](https://doi.org/10.1061/(ASCE)HY.1943-7900.0000772)
- Sarno L, Carravetta A, Martino R, et al. (2014) A two-layer depth-averaged approach to describe the regime stratification in collapses of dry granular columns. *Physics of Fluids* 26(10): 103303. <https://doi.org/10.1063/1.4898563>
- Sarno L, Carravetta A, Martino R, et al. (2017) Some considerations on numerical schemes for treating hyperbolicity issues in two-layer models. *Advances in Water Resources* 100: 183-198. <https://doi.org/10.1016/j.advwatres.2016.12.014>
- Savage SB, Hutter K (1989) The motion of a finite mass of granular material down a rough incline. *Journal of Fluid Mechanics* 199: 177-215. <https://doi.org/10.1017/S0022112089000340>
- Shieh CL, Jan CD, Tsai YF (1996) A numerical simulation of debris flow and its application. *Natural Hazards* 13(1): 39-54. <https://doi.org/10.1007/bf00156505>
- Takahashi T (1991) *Debris Flow*. Balkema, Rotterdam.
- Takahashi T (2007) *Debris Flow Mechanics, Prediction and Countermeasures*. Taylor & Francis, London.
- Toro-Escobar C, Parker G, Paola C (1996) Transfer function for the deposition of poorly sorted gravel in response to streambed aggradation. *Journal of Hydraulic Research* 34(1): 35-53. <https://doi.org/10.1080/00221689609498763>
- Wei FQ, Xie H, Lopez JL, et al. (2000) Extraordinarily serious debris flow disasters in Venezuela in 1999 *Mountain Research* 18(6): 580-582. (In Chinese)
- Wu W, Wang SSY, Jia Y (2000) Nonuniform sediment transport in alluvial rivers. *Journal of Hydraulic Research* 38(6): 427-434. <https://doi.org/10.1080/00221680009498296>
- Wu W, Wang SSY (2008) One-dimensional explicit finite-volume model for sediment transport. *Journal of Hydraulic Research* 46(1): 87-98. <https://doi.org/10.1080/00221686.2008.9521846>
- Xia C, Cao Z, Pender G, et al. (2017) Numerical Algorithms for Solving Shallow Water Hydro-Sediment-Morphodynamic Equations. *Engineering Computations* 34(8): 28366-286. <https://doi.org/10.1108/ec-01-2016-0026>
- Xia J, Lin B, Falconer RA, et al. (2010) Modelling dam-break flows over mobile beds using a 2D coupled approach. *Advances in Water Resources* 33(2): 171-183. <https://doi.org/10.1016/j.advwatres.2009.11.004>
- Zanuttigh B, Lamberti A (2007) Instability and surge development in debris flows. *Reviews of Geophysics* 45(3): RG3006. <https://doi.org/10.1029/2005rg000175>
- Zhang R, Xie J (1993) *Sedimentation research in China-systematic selections*. China Water and Power Press, Beijing, China. (In Chinese)
- Zhang S, Duan J (2011) 1D finite volume model of unsteady flow over mobile bed. *Journal of Hydrology* 405(1-2): 57-68. <https://doi.org/10.1016/j.jhydrol.2011.05.010>